Geophys. J. Int. (2008) doi: 10.1111/j.1365-246X.2008.03852.x

FAST TRACK PAPER

Coseismic slip model of the 2007 August Pisco earthquake (Peru) as constrained by Wide Swath radar observations

Mahdi Motagh,[1] Rongjiang Wang,[1] Thomas R. Walter,[1] Roland Bürgmann,[2] Eric Fielding,[3] Jan Anderssohn[4] and Jochen Zschau[1]

[1]*Department of Earthquake Risk and Early Warning, GeoForschungsZentrum (GFZ), Potsdam, Germany*
[2]*Department of Earth and Planetary Science and Berkeley Seismological Laboratory, University of California, Berkeley,* CA 94720*, USA*
[3]*Jet Propulsion Laboratory, California Institute of Technology, Pasadena,* CA 91109*, USA*
[4]*Department of Remote Sensing, GeoForschungsZentrum (GFZ), Potsdam, Germany*

Accepted 2008 May 12. Received 2008 May 12; in original form 2008 January 22

SUMMARY

The Pisco earthquake (M_w 8.0; 2007 August 15) occurred offshore of Peru's southern coast at the subduction interface between the Nazca and South American plates. It ruptured a previously identified seismic gap along the Peruvian margin. We use Wide Swath InSAR observations acquired by the Envisat satellite in descending and ascending orbits to constrain coseismic slip distribution of this subduction earthquake. The data show movement of the coastal regions by as much as 85 cm in the line-of-sight of the satellite. Distributed-slip model indicates that the coseismic slip reaches values of about 5.5 m at a depth of ∼18–20 km. The slip is confined to less than 40 km depth, with most of the moment release located on the shallow parts of the interface above 30 km depth. The region with maximum coseismic slip in the InSAR model is located offshore, close to the seismic moment centroid location. The geodetic estimate of seismic moment is 1.23×10^{21} Nm (M_w 8.06), consistent with seismic estimates. The slip model inferred from the InSAR observations suggests that the Pisco earthquake ruptured only a portion of the seismic gap zone in Peru between 13.5° S and 14.5° S, hence there is still a significant seismic gap to the south of the 2007 event that has not experienced a large earthquake since at least 1687.

Key words: Radar interferometry; Earthquake source observations; Continental margins: convergent.

GJI Seismology

INTRODUCTION

On 2007 August 15, a destructive earthquake of M_w 8.0 struck offshore of southern Peru near the port of Pisco (Fig. 1a). It produced strong ground shaking along the Pacific coastline between the capital Lima and the Paracas Peninsula, causing casualties and destruction throughout coastal regions in southern Peru. According to a preliminary report, at least 500 people died, nearly 1000 injured and many more left homeless (www.eeri.org). The moment centroid of the main rupture, corresponding to underthrust faulting (strike 321°, dip 28°, rake 63°), was located offshore at 13.73° S and 77.04° W (centroid time: 23:41:57.9 GMT)—about 180 km south-southwest of Lima or 90 km west of Pisco (Fig. 1a), as determined by the Global CMT Project moment tensor solution (http://www.globalcmt.org/; Event ID. 200708152340A).

The regional tectonics in Peru is dominated by the ∼65 mm yr^{-1}, northeast-directed subduction of the Nazca plate beneath the South American plate (Minster & Jordan 1978; Angermann *et al.* 1999). The region has been the site of four large subduction earthquakes over the past century (Fig. 1a), including the 1942 (M_w 8.1), 1996 (M_w 7.7) and 2001 (M_w 8.4) earthquakes to the south of Pisco, and the 1974 (M_w 7.9) and the 1940 (M_w 8.1) earthquakes to its north (Swenson & Beck 1999; Salichon *et al.* 2003; Pritchard *et al.* 2007). Previous studies identified the segment of the Nazca-South American plate boundary between the 1974 Lima event and those of 1942 and 1996 as a seismic gap that had not experienced a large earthquake since at least 1687 (Kelleher 1972; Dorbath *et al.* 1990; Swenson & Beck 1996; Swenson & Beck 1999). Therefore, the recent 2007 Pisco earthquake was the largest to strike within this ∼200-km-long gap in more than 300 yr. The use of InSAR data allows us to define a well-constrained slip model for the Pisco earthquake, providing insight to better assess the potential of the seismic gap to generate another large earthquake.

The Wide Swath mode of the Advanced Synthetic Aperture Radar (ASAR) sensor aboard the Envisat satellite has the potential to sample surface deformation over a 400-km-wide track roughly every 100 m (Fielding *et al.* 2007; Simons & Rosen 2007), as opposed to the ∼100-km-wide swaths of standard InSAR acquisitions. This

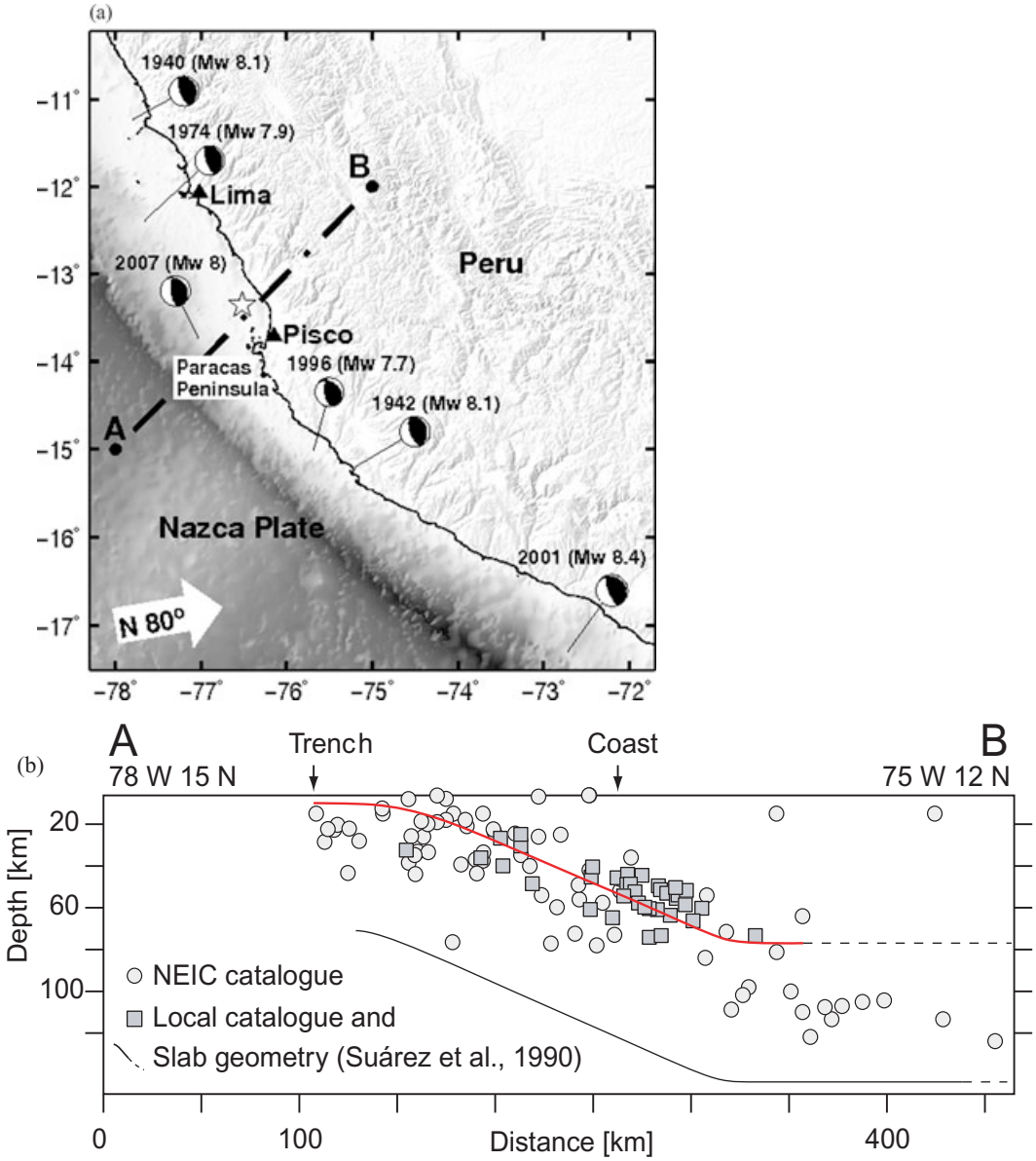

Figure 1. (a) Map of Nazca-South American subduction zone. Beach balls show the focal mechanism for large underthrusting earthquakes that occurred along the Peru subduction zone near Pisco during the past century (Dorbath *et al.* 1990; Swenson & Beck 1999; Pritchard *et al.* 2007). White star represents the hypocentre of the Pisco earthquake as determined by the USGS. The white arrow shows plate convergence direction (Minster & Jordan 1978; Angermann *et al.* 1999). (b) The geometry of the subducted slab beneath Peru as inferred by distribution of seismicity. Circles (NEIC) and squares (local catalogue) are epicentres of earthquakes with $M_w > 3$, occurred within 50 km of the profile A–B (Fig. 1a) during 1900–2007. The red line indicates the upper boundary of the subduction interface that we used to estimate coseismic slip distribution associated with the Pisco earthquake.

mode is hence of particular value for studies of subduction zone-related events that tend to span 100 s of km. In this study we use Wide Swath (WS) data acquired in descending and ascending orbits to derive detailed maps of the coseismic surface displacements caused by the 2007 August 15, Pisco earthquake. We invert these observations using a grid of rectangular dislocations in an elastic half-space (Okada 1985) for a distributed slip model of this subduction event.

WIDE SWATH INSAR DATA

The epicentral area of the Pisco earthquake was imaged by recent acquisitions of the Envisat satellite in Wide Swath mode on both ascending and descending tracks. We processed, using the SARscape software, four coseismic interferograms with favourable perpendicular baselines and burst coverage spanning the 2007 earthquake (Table 1): one from an ascending track (447); and the other three from a descending track (311). We use a 3 arcsec digital elevation model from the Shuttle Radar Topography Mission (Farr & Kobrick 2000) to account for topographic phase contributions and geocode the interferograms at 90 m resolution. We rely on precise obits from Envisat DORIS (http://ids.cls.fr) to model and remove the phase caused by the orbital separation of the two images and the topography. The interferograms were filtered using an adaptive power-spectrum filter (Goldstein & Werner 1998) and unwrapped using the Snaphu software (Chen & Zebker 2001).

Table 1. Wide-Swath interferograms constructed for this study.

	Track	Orbit	Date 1	Date 2	MBS* %	B_{Perp} (m)
Ifm_d1	311	24914–28922	2006/12/05	2007/09/11	77.24	~ -94
Ifm_d2	311	24914–29423	2006/12/05	2007/10/16	44.57	~ 62
Ifm_d3	311	24914–29924	2006/12/05	2007/11/20	52.00	~ 48
Ifm_a1	447	26052–29058	2007/02/23	2007/09/21	97.5	~ -2

MBS*: Minimum Burst Synchronization.

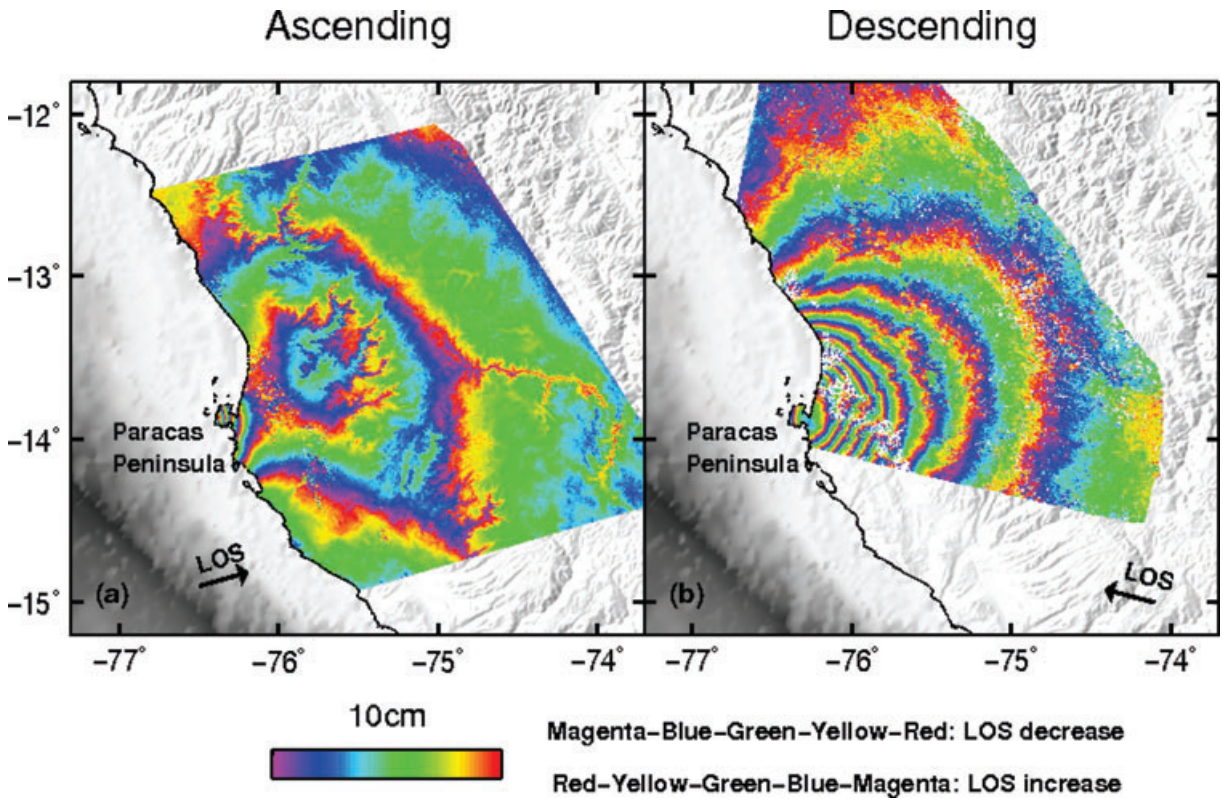

Figure 2. Wide Swath interferometric data used in this study. (a) Ascending interferogram. (b) Descending interferogram. Data are unwrapped, then rewrapped and plotted with each fringe representing 10 cm of line-of-sight displacement.

Figs 2(a) and (b) present the two best interferograms from the ascending and descending orbits, respectively, that were chosen for this study; the descending pairs ifm_d1 and ifm_d2 (Table 1) were noisier than ifm_d3 due to atmospheric perturbations and hence are not used here (Supplementary Material, Figs S1 and S2). Each interferogram shows the component of the three-dimensional displacement field in the satellite line-of-sight (LOS), whose incidence angle ranges from $\sim 16^\circ$ to 38° and from $\sim 18^\circ$ to 42° off vertical across descending and ascending tracks, respectively. The east-looking ascending interferogram shows slant range decreases, corresponding to motion of the ground towards the satellite (Fig. 2a). The peak LOS displacement occurs at the Paracas Peninsula, where it reaches up to 58 cm. To the east of the peninsula, the ascending interferogram exhibits some anomalous range decreases, several kilometres in extent, correlated with topographic relief that we assume to be a consequence of atmospheric perturbation sustained by radar signal. In contrast to the ascending interferogram, the interferometric phase in the descending interferogram is less disturbed (Fig. 2b). We infer up to 85 cm of slant range increase near the coast, corresponding to motion of the ground away from the satellite. The descending interferogram, however, has a reversal in the fringe pattern on the Paracas Peninsula, approximately in the same location where the ascending interferogram shows a prominent fringe gradient. This indicates that the vertical motion is changing sign there from subsidence to the east to uplift to the west. Ascending and descending interferograms are both consistent with the southwest-directed thrusting of the South America plate over the Nazca plate.

The two coseismic interferograms used in this study contain time periods several weeks to months before (master image) and after (slave) the earthquake. Therefore, they may encompass not only coseismic but also interseismic and post-seismic deformation. The interseismic signal, however, is expected to be negligible as previous GPS measurements suggest ~ 15 mm yr^{-1} of shortening parallel to the convergence direction across the fold and thrust belt in Peru (Norabuena *et al.* 1998). This corresponds to <5 mm of motion in the LOS direction in the <1-yr interferograms, which is less than the estimated uncertainty of the InSAR data. Post-seismic interferometric pairs do not show large-scale displacements, (Supplementary Material, Figs S3 and S4), although we observe a localized phase pattern around the Paracas Peninsula with less than 2 cm of range change for the time period 2007 September–October, and 2007 September–November. This signal, however, is difficult to differentiate from the short wavelength atmospheric distortion or orbital artefacts. Therefore, we

did not account for post-seismic or interseismic correction in our analysis. We presume that contributions from early post-seismic deformation transients, if any, constitute only a minor fraction of the observed coseismic signal (Simons *et al.* 2002; Pritchard *et al.* 2007).

SLIP DISTRIBUTION MODEL

To solve for the slip distribution that best describes the observed deformation, we first constrain the geometry of the subduction fault by using the location of the trench and distribution of seismicity (Fig. 1b). The fault dimension extends 300 km along strike and 160 km in the downdip direction to match the geographic extent of the earthquake's ground shaking (http://earthquake.usgs.gov) and depth of the locked interface (∼50 km) at the Peruvian margin (Norabuena *et al.* 1998). It is discretized into 5 × 5 km patches (1920 elements) for distributed slip inversion. The dip angle of fault patches varies from 8° at the trench to 27° at 50-km depth, consistent with the distribution of seismicity (Suarez *et al.* 1990), and GPS observations of Nazca-South American oblique convergence (Norabuena *et al.* 1998)—inversion tests using constant dip angle give results that differ substantially from those obtained using a curved geometry (Supplementary Material, Figs S5 and S6).

We use an elastic half-space model (Okada 1985) to calculate Green's function for each patch and utilize a sensitivity-based iterative method (Wang *et al.* 2008) to derive the slip distribution from the InSAR data. In this method, each fault patch is first examined to determine its greatest potential contribution to the observed surface deformation, measured by its contribution to the rms variance reduction ($\Delta\sigma$) of the data. As the major rupture area is likely to be associated with a larger $\Delta\sigma$ value than elsewhere, we assume that the slip at a fault patch is roughly correlated with its $\Delta\sigma$ value and so a first-order approximation of the slip pattern over the whole fault plane is obtained. To achieve a satisfactory compromise between stability and resolution, the variance reduction used is weighted by a sensitivity factor, which is expressed as a certain power of the modulus of Green's functions. The least-squares method is then used to scale the slip amplitude, resulting in a first-order slip model. To obtain higher-order approximations, the same fitting process is applied to the residual data, with the resulting slip distribution serving as a correction added to the previous slip model. The process is then repeated until the rms variance of the residual data decreases to a required minimum. A description of the methodology was presented in (Wang *et al.* 2008); more detail on the method and the software will be published separately.

To increase the computational efficiency, InSAR data are subsampled at a 450 m spacing within 5 km of the Paracas Peninsula, 900 m spacing within 5–10 km, ∼3 km spacing within 10–30 km of the peninsula, and ∼9 km spacing elsewhere, reducing the dataset from ∼12 millions to ∼55 000 points. We use location-dependent look angle to account for the varying LOS unit vector across the Wide Swath scene. The slip is constrained to only allow reverse faulting and left-lateral motion, consistent with the oblique convergence of the Nazca and South American plates (Minster & Jordan 1978; Angermann *et al.* 1999) and focal mechanism of the 2007 Pisco earthquake (http://www.globalcmt.org/).

The coseismic slip distribution constrained by descending and ascending interferograms is shown in Fig. 3. The slip model has two regions of concentrated slip: one with a peak amplitude of ∼5 m beneath the peninsula at about 30 km depth and the other offshore with about 5.5 m of slip at a depth of ∼18–20 km. In

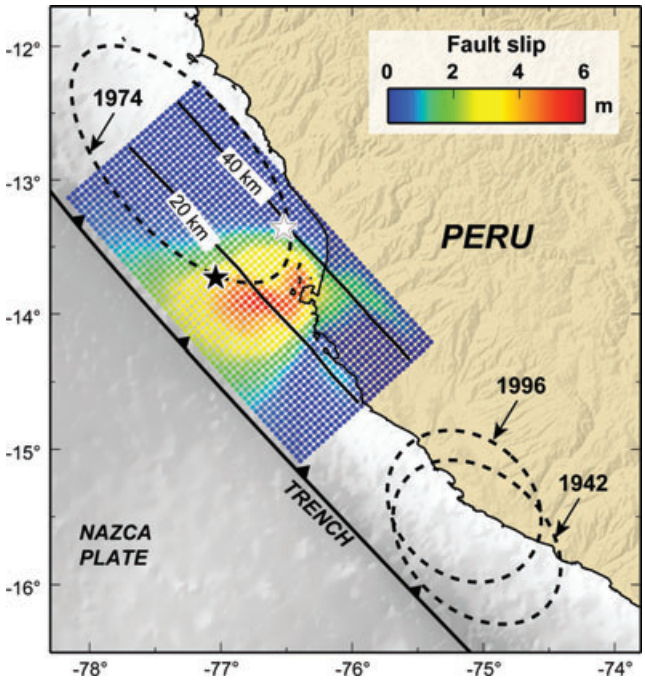

Figure 3. Slip distribution model for the 2007 Pisco earthquake constrained by InSAR data. The slip model is superimposed on shaded topography and bathymetry image. White and Black stars represent the locations of the Pisco earthquake as determined by the USGS and Global CMT Project, respectively. Ellipses represent approximate rupture areas of large underthrusting earthquakes that occurred along the Peru subduction zone near Pisco during the past century (Dorbath *et al.* 1990; Swenson & Beck 1999). The thick black lines in the slip model indicate depth of the subduction interface at 20-km interval.

general, the lateral edges and lower boundary of the slip are well resolved, but its upper edge is poorly constrained due to its distance from the observation data. The slip is confined to less than 40 km depth, with most of the slip occurring on the shallow part of the plate interface above 30 km depth (Fig. 3).

Figs 4(b) and (e) illustrate the predicted InSAR data for the best-fitting slip model shown in Fig. 3. The upper panel corresponds to the ascending interferogram and the bottom panel to the descending interferogram. Figs 4(c) and (f) show the residual interferograms formed by subtracting best-fitting models from the observed data. The RMS misfit for both ascending and descending interferograms is ∼3 cm. The residuals are almost flat—in particular, around the peninsula where InSAR exhibits maximum displacements, showing that our slip model well reproduces the InSAR observations. The majority of residuals are likely caused by either early post-seismic slip on the downdip portion of the main rupture or changes in tropospheric water vapour concentration between the two image acquisitions. The latter, in particular, appears to be the dominant factor in the ascending interferogram, resulting in perturbations of a few cm in the residual plots that are highly correlated with topographic elevation as expected for stably stratified troposphere (Supplementary Material, Fig. S7).

DISCUSSION AND CONCLUSIONS

This paper presents the use of WS SAR data acquired by the Envisat satellite during ascending and descending passes to constrain the slip model of a large earthquake. As shown here, WS-InSAR

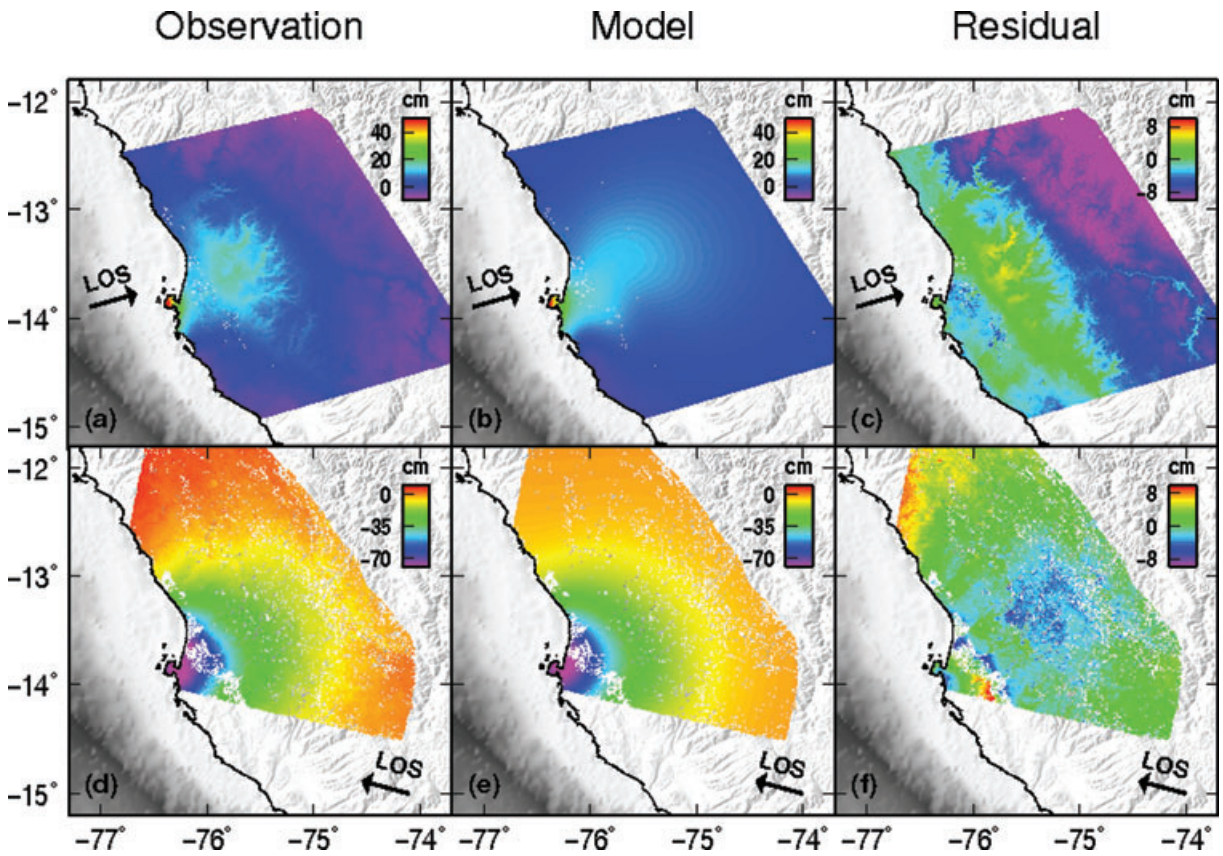

Figure 4. Observed and modeled InSAR data for the Pisco earthquake. The upper panel corresponds to the ascending interferogram and the lower panel to the descending interferogram. (a) and (d) LOS displacements. (b) and (e) Best-fitting models predicted by the distributed slip model in Fig. 3. (c) and (f) Residuals after subtracting best-fitting model prediction from the data. Black arrows indicate direction of satellite line-of-sight (LOS) vector.

is a powerful imaging tool that significantly improves our ability to derive detailed deformation maps of major events and is very promising for studies of continental-scale tectonics where deformation fields tend to span 100 s of km. The InSAR-derived slip model of the 2007 Pisco earthquake suggests that the slip is confined to the uppermost 40 km of the subduction interface with a peak amplitude of about 5.5 m of slip at a depth of ∼20 km. The total geodetic moment estimated from InSAR is 1.23×10^{21} Nm (M_w 8.06), somewhat larger than the CMT estimate of 1.12×10^{21} Nm (M_w 8). The difference may be due to a number of factors including contributions from early post-seismic deformation to the geodetic data, assumptions about the elastic moduli used in the moment estimate, or an overestimate of slip far offshore.

Preliminary inversion of the waveform data from the Global Seismographic Network (GSN), suggests a heterogeneous slip model for the Pisco earthquake with a rupture extent of ∼200 km and two zones of high-slip (known as asperities) located offshore (Fig. 5a)—one to the south of the Paracas Peninsula with 8 m of slip and the other to its north with as much as 4 m of slip (Chen Ji and Yuehua Zeng at the USGS and UCSB: http://earthquake.usgs.gov/eqcenter/eqinthenews/2007/us2007gbcv/finite_fault.php). Inversion of P and SH waves from the Federation of Digital Seismograph Networks (FDSN), suggests a rupture extent of ∼120 km with two asperities (Fig. 5b) similar in form to the GSN results—a large asperity zone to the west of the Paracas Peninsula with 6 m of slip and another smaller asperity to the north of the peninsula with ∼3 m of slip (http://geoazur.unice.fr/SEISME/PERU150807/note1.html).

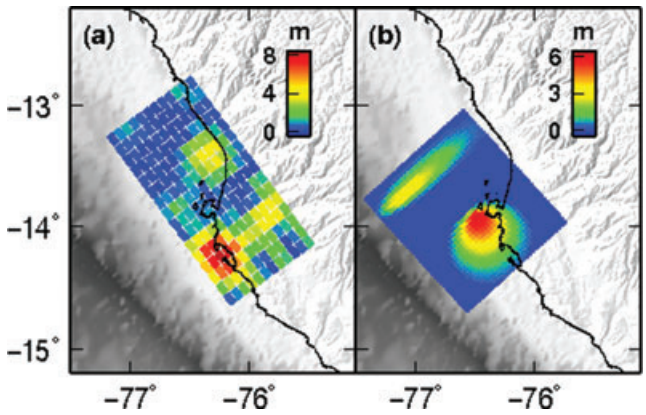

Figure 5. Distributed slip models from teleseismic observations. (a) Estimated slip distribution from the inversion of the Global Seismographic Network (GSN) waveform data provided by USGS (Chen Ji and Yuehua Zeng at the USGS and UCSB: http://earthquake.usgs.gov/eqcenter/eqinthenews/2007/us2007gbcv/finite_fault.php). (b) Estimated slip distribution from the inversion of the Federation of Digital Seismograph Networks (FDSN) waveform data provided by Geosciences Azur (http://geoazur.unice.fr/SEISME/PERU150807/note1.html).

InSAR observations show a different picture of the slip distribution associated with the Pisco earthquake from those suggested by the early teleseismic inversions. The InSAR data require a single contiguous deforming zone on the subduction interface with two linked asperities occurring offshore. The USGS-NEIC hypocentre

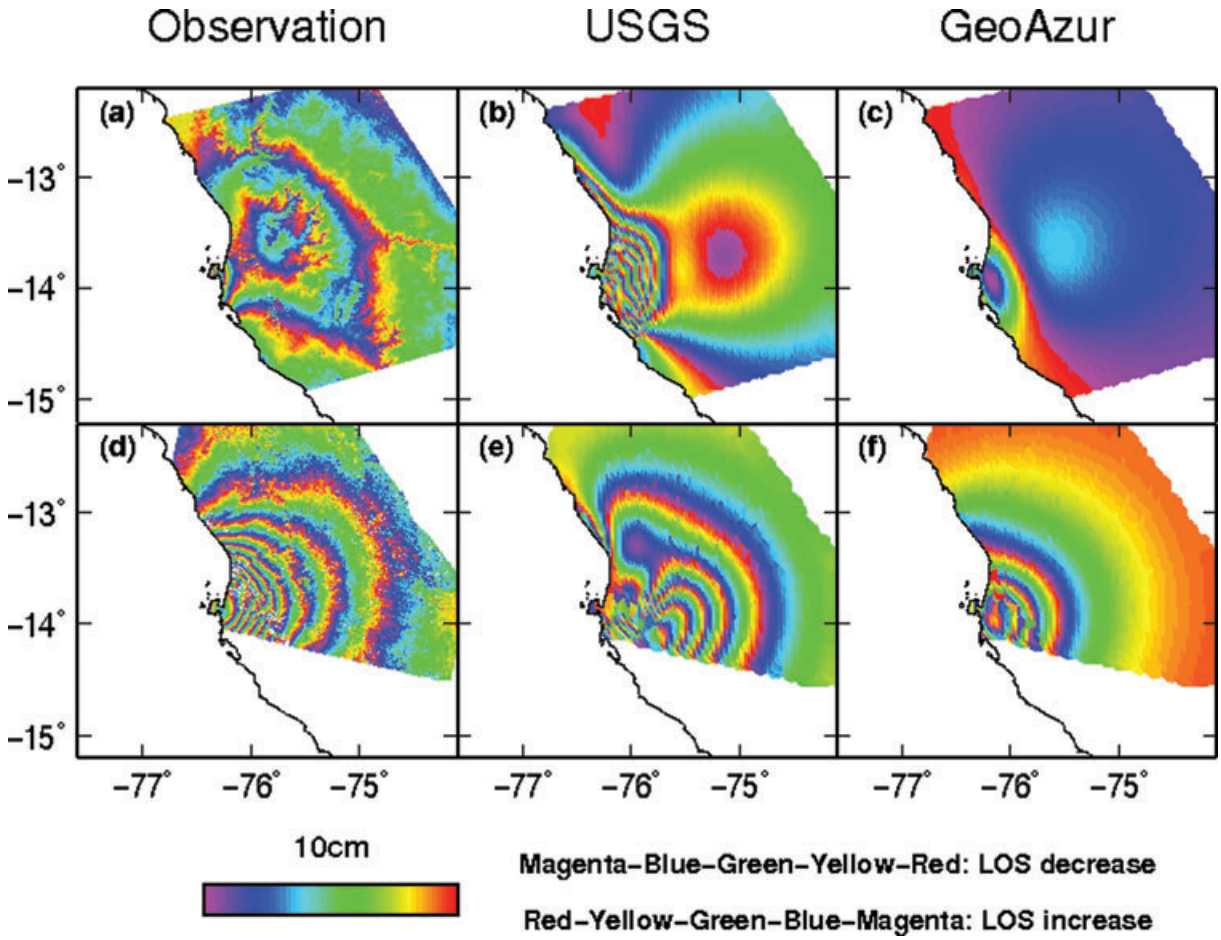

Figure 6. Synthetic interferograms for teleseismic slip models. (a) Ascending interferogram. (b) Synthetic ascending interferogram for the teleseismic model shown in Fig. 5a. (c) Synthetic ascending interferogram for the teleseismic model shown in Fig. 5(b). (d–f) Similar to (a–c), but for the descending geometry.

is located near the downdip limit of the rupture zone, while the Harvard CMT (black star in Fig. 3a) is close to area of peak slip at depths of 18–20 km. This may be interpreted in terms of a dominantly up-dip propagation of the coseismic rupture front. InSAR observations do not support a large separation of two asperities as suggested by teleseismic results.

Moreover, we find that the teleseismic models do not fully explain the InSAR data. Fig. 6 shows the observed and predicted LOS measurements from the teleseismic slip models. For the ascending geometry, the GSN model from the USGS (Fig. 6b) overestimates substantially LOS data around the peninsula, while the FDSN model from GeoAzur (Fig. 6c) underestimates InSAR observations. For the descending geometry, while both models predict the correct direction of surface motion, they underestimate the amount of LOS displacement observed by InSAR (Figs 6e,f). A joint inversion of geodetic and seismic data would, therefore, be necessary to better constrain earthquake rupture properties and reconcile discrepancies arising from independent observations (Pritchard & Fielding 2008).

The 2007 Pisco earthquake ruptured part of a known seismic gap along the Peruvian margin between the 1974 event and those in 1942 and 1996, but only partially filled this gap. A comparison between the rupture extent of the 2007 event obtained by InSAR and those in 1974, 1942 and 1996 suggests a significant gap southeast of the 2007 rupture that has not failed since 1687 (Fig. 3). Hence, the area to the south of the Paracas Peninsula, between the southeastern-most extent of the 2007 rupture and the northwestern-most extent of the 1942 and 1996 ruptures, still has the potential for a large earthquake in the future.

ACKNOWLEDGMENTS

This work was supported by the German Research Foundation (DFG) through a research fellowship to Mahdi Motagh (MO 1851/1-1). Part of the research described in this paper was carried out at the Jet Propulsion Laboratory (JPL), California Institute of Technology, under a contract with NASA. Some of the figures were prepared using the public domain GMT software (Wessel & Smith 1998). We thank Martin Vallée for providing us with his slip model, Manoochehr Shirzaei for discussions and Kevin Fleming for his comments on the manuscript. We are grateful to Kaj Johnson and an anonymous reviewer for their thoughtful review and appreciate constructive comments by the Editor, John Beavan. Envisat wide swath data were provided by the European Space Agency via category-1 proposal AOALO 3740.

REFERENCES

Angermann, D., Klotz, J. & Reigber, C., 1999. Space-geodetic estimation of the Nazca-South America Euler vector, *Earth. Planet. Sci. Lett.*, **171,** 329–334.

Chen, C. W. & Zebker, H. A., 2001. Two-dimensional phase unwrapping with use of statistical models for cost functions in nonlinear optimization, *J. Opt. Soc. Am. A*, **18**(2), 338–351.

Dorbath, L., Cisternas, A. & Dorbath, C., 1990. Assessment of the size of large and great historical earthquakes in Peru, *Bull. seism. Soc. Am.*, **80**(3), 551–576.

Farr, T. G. & Kobrick, M., 2000. The Shuttle Radar Topography Mission produces a wealth of data, *EOS Trans. AGU*, **81,** 583–585.

Fielding, E. J., Rosen, P. A. & Bürgmann, R., 2007. Large-scale deformation of Tibet measured with Envisat ScanSAR interferometry, *Eos Trans. AGU, Suppl.* **88**(52).

Goldstein, R. M. & Werner, C. L., 1998. Radar interferogram filtering for geophysical applications, *Geophys. Res. Lett.*, **25**(21), 4035–4038.

Kelleher, J. A., 1972. Rupture zones of large South American earthquakes and some predictions, *J. geophys. Res.*, **77**(11), 2087–2103.

Minster, J. B. & Jordan, T. H., 1978. Present-day plate motions, *J. geophys. Res.*, **83**(B11), 5331–5354.

Norabuena, E., Leffler, G. L., Mao, A., Dixon, T., Stein, S., Sacks, I. S., Ocola, L. & Ellis, M., 1998. Space geodetic observations of Nazca-South America convergence across the Central Andes, *Science*, **279**(5349), 358–362.

Okada, Y., 1985. Surface deformation due to shear and tensile faults in a half-space, *Bull. seism. Soc. Am.*, **75,** 1135–1154.

Pritchard, M. E. & Fielding, E. J., 2008. A study of the 2006 and 2007 earthquake sequence of Pisco, Peru, with InSAR and teleseismic data, *Geophys. Res. Lett.*, **35,** L09308, doi:10.1029/2008GL033374.

Pritchard, M. E., Norabuena, E. O., Ji, C., Boroschek, R., Comte, D., Simons, M., Dixon, T. H. & Rosen, P. A., 2007. Geodetic, teleseismic, and strong motion constraints on slip from recent southern Peru subduction zone earthquakes, *J. geophys. Res.*, **112**(B3), 1–24.

Salichon, J., Delouis, B., Lundgren, P., Giardini, D., Costantini, M. & Rosen, P., 2003. Joint inversion of broadband teleseismic and interferometric synthetic aperture radar (InSAR) data for the slip history of the M_w = 7.7, Nazca ridge (Peru) earthquake of 12 November 1996, *J. geophys. Res.*, **108**(B2), 2085, doi:10.1029/2001JB000913.

Simons, M., Fialko, Y. & Rivera, L., 2002. Coseismic deformation from the 1999 M_w 7.1 Hector Mine, California, earthquake as inferred from InSAR and GPS observations, *Bull. seism. Soc. Am.*, **92**(4), 1390–1402.

Simons, M. & Rosen, P., 2007. Interferometric synthetic aperture radar geodesy, in *Treatise on Geophysics*, Schubert, G., ed., Vol. 3. pp. 391–446. Geodesy, Elsevier Press, Amsterdam.

Suarez, G., Gagnepain, J., Cisternas, A., Hatzfeld, D., Molnar, P., Ocola, L., Roecker, S. W. & Viode, J. P., 1990. Tectonic deformation of the Andes and the configuration of the subducted slab in central Peru; results from a microseismic experiment, *Geophys. J. Int.,* **103**(1), 1–12.

Swenson, J. L. & Beck, S. L., 1996. Historical 1942 Ecuador and 1942 Peru subduction earthquakes, and earthquake cycles along Colombia-Ecuador and Peru subduction segments, *Pure appl. Geophys*, **146**(1), 67–101.

Swenson, J. L. & Beck, S. L., 1999. Source characteristics of the 12 November 1996M_w 7.7 Peru subduction zone earthquake, *Pure appl. Geophys*, **154,** 731–751.

Wang, R., Motagh, M. & Walter, T. R., 2008. Inversion of slip distribution from co-seismic deformation data by a sensitivity-based iterative fitting method, *EGU General Assembly 2008*, EGU2008-A-07971.

Wessel, P. & Smith, W. H. F., 1998. New improved version of generic mapping tools released, *Eos Trans. AGU*, **79**(47), 579.

SUPPORTING INFORMATION

Additional Supporting Information may be found in the online version of this article.

Appendix S1. Supplementary Figs S1–S7 referenced in the text (PDF format).

Please note: Blackwell Publishing are not responsible for the content or functionality of any supporting materials supplied by the authors. Any queries (other than missing material) should be directed to the corresponding author for the article.